



HHS Public Access

Author manuscript

Biochem Pharmacol. Author manuscript; available in PMC 2022 October 01.

Published in final edited form as:

Biochem Pharmacol. 2021 October ; 192: 114739. doi:10.1016/j.bcp.2021.114739.

Adenosine A₁ Receptor is Dispensable for Hepatocyte Glucose Metabolism and Insulin Sensitivity

Shanu Jain¹, Luiz F. Barella², Jürgen Wess², Marc L. Reitman³, Kenneth A. Jacobson¹

¹Molecular Recognition Section, Laboratory of Bioorganic Chemistry, National Institute of Diabetes and Digestive and Kidney Diseases, Bethesda, MD 20892, USA.

²Molecular Signaling Section, Laboratory of Bioorganic Chemistry, National Institute of Diabetes and Digestive and Kidney Diseases, Bethesda, MD 20892, USA.

³Diabetes, Endocrinology, and Obesity Branch, National Institute of Diabetes and Digestive and Kidney Diseases, NIH, Bethesda, MD 20892, USA.

Abstract

Hepatic insulin resistance (IR) and enhanced hepatic glucose production (HGP) are key features of type 2 diabetes (T2D), contributing to fasting hyperglycemia. Adenosine receptors (ARs) are G protein-coupled and expressed in hepatocytes. Here, we explored the role of hepatic G_{i/o}-coupled A₁AR on insulin resistance and glucose fluxes associated with obesity. We generated a mouse model with hepatocyte-specific deletion of A₁AR (A1L^{-/-}), which was compared with whole body knockout of A₁AR or A₁AR/A₃AR (both G_i-coupled). Selective deletion of hepatic A₁AR resulted in a modest improvement in insulin sensitivity. In addition, HFD A1L^{-/-} mice showed decreased fasting glucose levels. Hyperinsulinemic-euglycemic clamp studies demonstrated enhanced insulin sensitivity with no change in HGP in HFD A1L^{-/-} mice. Similar to A1L^{-/-}, fasting blood glucose levels were significantly reduced in whole body A1^{-/-} and A1^{-/-}A3^{-/-} compared to wild-type mice. Taken together, our data support the concept that blocking hepatic A₁AR may decrease fasting blood glucose levels without directly affecting hepatocyte glucose metabolism and insulin sensitivity.

Graphical Abstract

Authorship Contributions:

Participated in research design: SJ, KAJ, JW, MLR

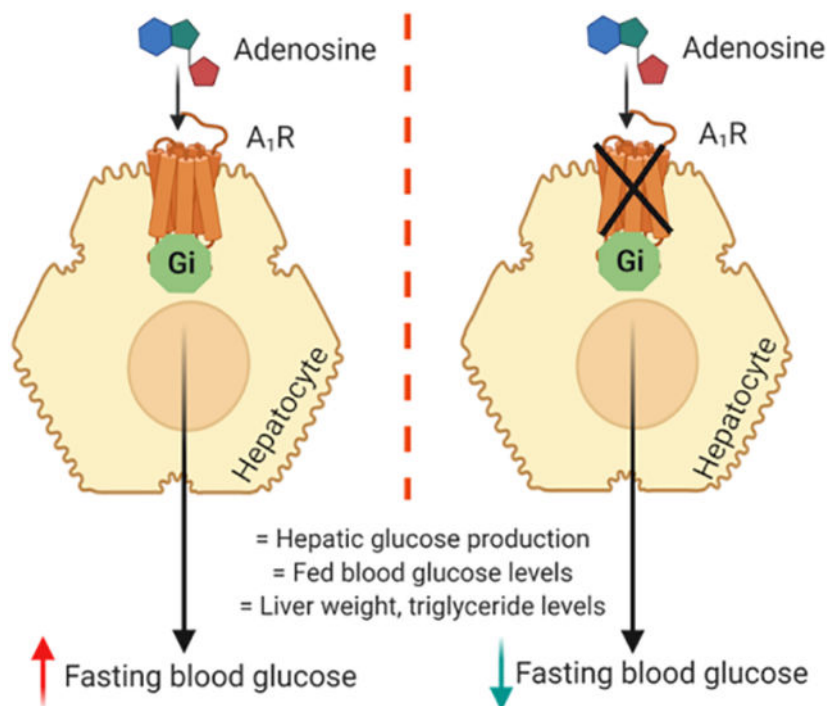
Conducted experiments: SJ, LFB

Performed data analysis: SJ

Wrote or contributed to the writing of the manuscript: SJ, KAJ, JW, MLR

Conflict of interest statement: The authors declare no conflict of interest.

Publisher's Disclaimer: This is a PDF file of an unedited manuscript that has been accepted for publication. As a service to our customers we are providing this early version of the manuscript. The manuscript will undergo copyediting, typesetting, and review of the resulting proof before it is published in its final form. Please note that during the production process errors may be discovered which could affect the content, and all legal disclaimers that apply to the journal pertain.



Keywords

G protein-coupled receptor; liver; adenosine; diabetes; obesity; glucose metabolism

1. INTRODUCTION

One key characteristic element of type 2 diabetes (T2D) is the dysregulation of hepatic processes that are crucial for the maintenance of normal glucose homeostasis [1]. Post-prandially, the liver contributes to glucose disposal by increasing the rates of glycogen and fatty acid synthesis [2]. During fasting, the liver plays a central role in maintaining blood glucose levels by increasing gluconeogenesis and glycogenolysis, promoting hepatic glucose production (HGP) [3]. These processes maintain euglycemia, providing fuel to glucose-consuming cells including neurons, red blood cells and renal medullary cells. In T2D, hepatic insulin resistance enhances HGP rates contributing to hyperglycemia [4, 5]. Obesity-induced insulin resistance also increases circulating free fatty acid (FFA) levels, which along with hepatic de-novo lipogenesis cause liver steatosis that can progress to steatohepatitis and fibrosis [6, 7]. Hence, the identification of factors that control liver glucose metabolism and insulin sensitivity is needed in order to develop new strategies to interfere with these pathophysiological processes.

Extracellular adenosine exerts its range of cellular responses through binding and activating four G protein-coupled receptors (GPCRs), A₁, A_{2A}, A_{2B} and A₃ adenosine receptors (ARs) [8, 9]. All four ARs are expressed in hepatocytes [10]. Involvement of ARs in the regulation of glucose homeostasis and diabetes mellitus has been demonstrated previously, but the roles of AR subtypes in a tissue-specific manner are unclear [11–14]. In liver, infused adenosine

mildly attenuates insulin's suppression of HGP and, therefore, increases blood glucose levels [15]. This increase in hepatic glycogenolysis is mediated via G_i -coupled A_1AR activation in a Ca^{2+} -dependent manner [16]. Another study found that hepatic lipogenesis and steatosis were increased due to A_1AR activation in ethanol-induced fatty liver. Mice lacking the A_1AR were protected from developing ethanol-induced steatosis [17], with A_1AR associated with fatty acid (FA) synthesis. This is the first study to generate a hepatocyte-specific A_1AR knockout mouse model to understand the receptor's involvement in high fat diet (HFD)-induced hepatic insulin resistance and hepatic glucose fluxes. Our results indicate that lack of A_1AR in hepatocytes ($A1L^{-/-}$) did not affect hepatic glucose metabolism and insulin sensitivity. However, the $A1L^{-/-}$ mice displayed decreased fasting glucose levels and improved whole-body insulin sensitivity probably due to indirect effects on other metabolic tissues. Future studies are required to unravel the indirect mechanistic effects of hepatic A_1AR on whole body metabolism.

2. MATERIALS AND METHODS

2.1. Mouse models

To selectively delete A_1AR in hepatocytes, 8-week-old mice with an A_1AR -floxed gene ($A1f/f$, provided by Dr. Robert Greene, Univ. of Texas Southwestern Medical Center, Dallas, TX) [18] were injected with either AAV-TBG-EGFP or AAV-TBG-CRE virus (1×10^{11} infectious particles) via the tail vein in 100 μ l saline solution. Recombinant adeno-associated viruses (AAVs) coding for enhanced green fluorescent protein (EGFP) (AAV-TBG-EGFP) or Cre recombinase (AAV-TBG-CRE) were obtained from the Vector Core of the University of Pennsylvania (Philadelphia, PA). Expression of Cre recombinase is under the control of hepatocyte-selective thyroxine-binding globulin (TBG) promoter, and hence Cre recombinase is selectively expressed in hepatocytes. AAV-TBG-EGFP, coding for EGFP, was used to generate control mice.

The A_1 - A_3AR double knockout mice ($A1^{-/-}A3^{-/-}$) were bred from the individual knockout mice as we reported [19–21]. $A1A3^{-/-}$ were bred with wild-type (WT) C57BL/6J mice (Taconic Biosciences, Rensselaer, NY) to generate double heterozygous $A1^{+/+}A3^{+/+}$ animals. The interbreeding of $A1^{+/+}A3^{+/+}$ mice generated experimental mice comprising double knockout ($A1^{-/-}A3^{-/-}$), A_1AR knockout ($A1^{-/-}$), A_3AR knockout ($A3^{-/-}$) and WT ($A1^{+/+}A3^{+/+}$) mice. The breeding of double heterozygous pairs indicated deviation of genotype distribution from a Mendelian ratio in the weaned pups. The mice pups with $A1^{-/-}$ and $A1^{-/-}A3^{-/-}$ were significantly reduced in number compared to $A3^{-/-}$ and $A1^{+/+}A3^{+/+}$ mice. Lack of A_1AR may cause prenatal lethality resulting in the skewed genotype distribution observed in our study. All experiments were carried out using male littermates.

2.2. Mouse maintenance and diet

Mice were housed on a 12-h light/12-h dark cycle in a pathogen-free barrier facility at room temperature (23 °C). The mice had ad libitum access to water. The mice were maintained on standard mouse chow (7022 NIH-07 diet, 15% kcal fat, energy density 3.1 kcal/g, Envigo, Inc., Indianapolis, IN) or a HFD (36% fat, equivalent to 60% kcal; 36% carbohydrate; F3282; Bio-Serv, Flemington, NJ).

2.3. In vivo metabolic tests

Unless indicated, the source of reagent grade chemicals is Sigma-Aldrich (St. Louis, MO). Metabolic phenotyping was carried out on mice fed a chow diet (CD) or a HFD [22]. Tests were initiated when mice reached the age of 8 weeks. A glucose tolerance test (GTT) was carried out on mice fasted overnight for 12 h. Glucose (1 (HFD) or 2 (CD) g/kg) was injected intraperitoneally (i.p.), and blood glucose concentrations were determined using blood from the tail vein immediately before (0 min) and after administration at 15, 30, 60, 90 and 120 min. Blood glucose levels were determined using a glucometer (Bayer Contour glucometer, Contour Plus). An insulin tolerance test (ITT-4 h fasted mice) and a pyruvate tolerance test (PTT-overnight fasted mice) were conducted by i.p. injection of human insulin (0.75 (CD) or 1 (HFD) U/kg; Humulin, Eli Lilly) or sodium pyruvate (2 g/kg), respectively, as indicated. Blood glucose concentrations were determined at 15, 30, 60, 90 and 120 min after injection. A glucagon challenge test (GCT) was conducted by i.p. injecting 16 µg/kg of glucagon, and blood glucose levels were determined at specific time points.

2.4. Hyperinsulinemic-euglycemic clamps

All procedures for the hyperinsulinemic–euglycemic clamp were conducted at Vanderbilt University’s Mouse Metabolic Phenotyping Center (Nashville, TN) and approved by the Vanderbilt University Animal Care and Use Committee. Catheters were implanted into a carotid artery and a jugular vein of the mice (Male, AIL⁺ and control mice, C57BL/6) for sampling and infusions, respectively, five days before the study, as described by Berglund et al. [23]. Insulin clamps were performed on 5 h-fasted conscious, unhandled mice, using a modification of the method described by Ayala et al. [24]. After 3 h of fast, an arterial blood sample was obtained to determine natural isotopic enrichment of plasma glucose. Immediately following this sample, a quantitative stable isotope delivery to increase isotopic enrichment above natural isotopic labelling was initiated as described previously [25]. Briefly, a [6,6-²H₂]glucose-²H₂O (99.9%)-saline bolus was infused for 25 min to enrich total body water to 4.5% (t = -120 min to -95 min). A continuous infusion of [6,6-²H₂]glucose (t = -95 min to 0 min; 0.8 mg kg⁻¹ min⁻¹) was started following the [6,6-²H₂]glucose-²H₂O-saline prime. The insulin clamp was initiated at t = 0 min with a continuous insulin infusion (4 mU/kg body weight/min). At the same time, a variable infusion of glucose was started (50% dextrose + ²H₂O (0.04 MPE) + [6,6-²H₂]glucose (0.08 MPE)) in order to maintain stable euglycemia and stable enrichment of ²H₂O and [6,6-²H₂]glucose in plasma. Washed red blood cells were also continuously infused during the clamp period to maintain hematocrit. Each infusate was prepared in a 4.5% ²H₂O-enriched saline solution. Arterial glucose levels were monitored every 10 min to provide feedback for adjustment of the glucose infusion rate (GIR). Steady state blood sampling for glucose kinetics was performed at t = -10 and t = 90–120 min of the clamp. Clamp insulin was determined at t = 120 min. At 120 min, 13 µCi of [¹⁴C]2-deoxyglucose ([¹⁴C]2DG) was administered as an intravenous bolus. Blood was taken from 2–25 min for determination of plasma [¹⁴C]2DG. At t = 145 min, mice were sacrificed by pentobarbital injection, and tissues immediately frozen in liquid nitrogen. Plasma glucose enrichments ([6,6-²H₂]glucose), isotopomer distribution and the enrichment ratio of deuterium on the fifth (C5) and second (C2) carbons of glucose were assessed by GC-MS as described previously [26]. Glucose fluxes were assessed using non–steady-state equations (volume of

distribution of glucose = 130 ml/kg) [27]. The contribution of gluconeogenesis was assessed as the ratio of C5 and C2 of plasma glucose [28, 29]. [¹⁴C]2DG in plasma samples and [¹⁴C]2DG-6-phosphate in tissue samples were determined by liquid scintillation counting. The glucose metabolic index (Rg) was calculated as previously described [30]. Plasma insulin was determined by RIA. Stable isotopes were purchased from Cambridge Isotope Laboratories, Inc. (Tewksbury, MA). Radioactive tracers were purchased from PerkinElmer (Boston, MA). Body composition was measured using a Bruker Minispec NMR (Bruker, Billerica, MA).

2.5. cDNA preparation and qRT-PCR

Mouse tissues were dissected and frozen immediately in liquid nitrogen. Total RNA was extracted using an RNeasy mini kit (Qiagen, Germantown, MD), as per the manufacturer's protocol. cDNA was synthesized using 1 µg of total RNA using Superscript III First Strand synthesis Super Mix (Invitrogen, Thermo Fisher, Rockville, MD). Quantitative real time PCR (qRT-PCR) was performed using the SYBR green reagent (Applied Biosystems, Beverly, MA) in triplicates. Primer sequences are provided in Table 1. Gene expression data were normalized to the relative expression of 18s rRNA using the Ct method.

2.6. Measurement of plasma insulin and glucagon levels

Blood was collected at 10 AM from the tail vein of ad libitum fed or 12-h fasted mice using EDTA-coated tubes (SAFE-T-FILL, RAM Scientific, Yonkers, NY). To measure glucagon, blood was collected in tubes supplemented with aprotinin (proteinase inhibitor) and DPP-4 inhibitor K579 ((S)-1-(4-methyl-1-(2-pyrimidinyl)-4-piperidylamino) acetyl-2-pyrrolidinedicarbonitrile, Sigma). Blood was centrifuged at 4°C at 12,000 × g for 10 min. Plasma insulin concentrations were measured using an ELISA kit (Crystal Chem, Inc., Elk Grove Village, IL) as per the manufacturer's instructions. Glucagon was assayed using a commercially available ELISA kit (Mercodia, Winston Salem, NC).

2.7. Body composition analysis

The lean/fat mass composition of knockout and control mice was measured using a 3-in-1 Echo Magnetic Resonance Imaging (MRI) Analyzer (Echo Medical Systems, Houston, TX).

2.8. Glycogen level and triglyceride estimation in liver tissues

For measuring glycogen levels, liver tissues (10 mg samples) were processed following the colorimetric method of a glycogen assay kit (Abnova, Walnut, CA). Liver triglyceride levels were measured by homogenizing 20 mg of tissue in phosphate buffered saline (PBS). A chloroform/methanol (2:1) mixture was added to the liver homogenate. The homogenate was centrifuged, and the organic phase was transferred to a new tube and dried overnight. Each sample was dissolved in ethanol containing 1% Triton X-100, and triglyceride levels were measured using a triglyceride reagent (product T2449, Sigma, St. Louis, MO). Triglyceride levels were normalized to protein levels in liver homogenates.

2.9. In-vivo insulin signaling

Mice on HFD were fasted for 5 h, anesthetized (isoflurane, inhaled), and the inferior vena cava was exposed. Human insulin (5U, Humulin, Eli Lilly) dissolved in 0.9% of saline (100 μ l) was injected into the vena cava [31]. Tissues were harvested 5 min after injections starting with liver, followed by adipose and skeletal muscle. Tissues were snap frozen for Western blot analysis.

2.10. Western blot studies

Western blot studies were carried out as described previously [32]. Briefly, adipocytes or adipose tissues were homogenized in adipocyte lysis buffer (50 mM Tris, pH 7.4, 500 mM NaCl, 1% nonyl phenoxypolyethoxyethanol (NP40), 20% glycerol, 5 mM EDTA, and 1 mM phenylmethylsulfonyl fluoride (PMSF)) supplemented with EDTA-free protease inhibitor cocktail and phosphatase inhibitors cocktail (Roche Diagnostics Corp., South San Francisco CA). Protein concentrations in the lysates were determined using a bicinchoninic acid (BCA) assay kit (Pierce, Rockford, IL). Protein was denatured in NuPAGE LDS sample buffer (Thermo Fisher Scientific, Waltham, MA) and β -mercaptoethanol at 90 °C for 5 min. Protein lysates were separated using 4–12% SDS-PAGE (Invitrogen, Carlsbad, CA) and transferred to nitrocellulose membranes (Bio-Rad, Hercules, CA). Membranes were incubated with primary antibody overnight at 4 °C in 5% w/v BSA prepared in 1x TBS with 0.1% Tween 20. On the next day, the membranes were washed and incubated with HRP-conjugated anti-rabbit/mouse secondary antibody. SuperSignal West Pico Chemiluminescent Substrate (Pierce, Rockford, IL) was used to visualize immunoreactive bands using an Azure Imager C600 (Azure Biosystems, Dublin, CA). Images were analyzed using ImageJ (NIH, Bethesda, MD). The antibodies (all purchased from Cell Signaling Technology, Danvers, MA, product number indicated) used for Western blots were: T-AKT, 9272; p-AKT (Ser473), 4060; β -actin, 4970.

2.11. Statistics

All data are expressed as the mean \pm SEM. Data were tested for statistical significance by 1- or 2-way ANOVA or by a 2-tailed, unpaired Student's *t* test, as appropriate. A *P* value <0.05 was considered significant. Post-hoc calculation of statistical power and effect size were undertaken for whole-body knockout datasets (Figure 6 and Figure 7). (<https://clincalc.com/stats/Power.aspx>).

2.12. Study approval

The study and its procedures were approved by the Animal Care and Use Committee of National Institute of Diabetes and Digestive and Kidney Diseases, animal protocol K083-LBC-17.

3. RESULTS

3.1. Generation of hepatocyte-specific A₁AR knockout mice (A1L^{-/-})

To generate a mouse model lacking A₁AR specifically in hepatocytes, we injected 8-week-old A₁AR-floxed mice with an adeno-associated virus (AAV8) coding for *Cre* recombinase

(AAV8-TBG-CRE) (1×10^{11} infectious particles in 100 μ l/mouse) via tail vein. A₁AR-floxed mice injected with an EGFP-encoding AAV8 (AAV8-TBG-EGFP) served as control animals. AAV8-TBG-CRE-injected A₁AR-floxed mice showed a nearly complete loss of liver A₁AR expression, while A₁AR mRNA levels remained unaffected in other major tissues (Figure 1A). This suggested that virtually all of the liver A₁AR expression is in hepatocytes.

3.2. Metabolic studies with A1L^{-/-} and control mice on chow diet (CD)

Metabolic tests were carried out with A1L^{-/-} and control mice maintained on CD two weeks after virus injection. Both mouse groups showed similar glucose tolerance (Figure 1B) and insulin sensitivity (AUC (A.U.)-ITT Control: 140.6 ± 21.86 ; A1L^{-/-} : 173.4 ± 25.71 (Figure 1C). Similarly, CD A1L^{-/-} and control mice showed similar blood glucose excursions in a PTT (Figure 1D). We also carried out a glucagon challenge test to examine the ability of glucagon to stimulate hepatic glucose output. Injection of glucagon (16 μ g/kg, i.p.) caused similar increases in blood glucose levels in CD A1L^{-/-} and control mice (Figure 1E).

Next, we examined blood glucose, plasma insulin, and glucagon levels. Fasting and fed blood glucose levels were similar in CD A1L^{-/-} and control mice (Figure 1F). Fasting plasma insulin levels were similar in the two groups, but fed insulin levels were significantly higher in A1L^{-/-} mice (Figure 1G). Circulating plasma glucagon levels were similar in the two mouse cohorts (Figure 1H). Taken together, the data show that hepatocyte A₁AR does not play a role in regulating liver glucose metabolism in CD fed conditions.

3.3. Metabolic studies with A1L^{-/-} and control mice on HFD

To determine the role of the hepatocyte A₁AR on diet-induced dysregulation of glucose metabolism, groups of A1L^{-/-} and control mice were challenged with a HFD starting two weeks after AAV injection. Body mass was recorded for the next 7 weeks on a HFD. A1L^{-/-} and control mice demonstrated similar weight gain when consuming a HFD (Figure 2A). Next, we subjected the mice to a series of metabolic tests after 8 weeks on a HFD. HFD A1L^{-/-} mice showed modestly improved glucose tolerance (Figures 2B, 2C) and improved insulin sensitivity (Figures 2D, 2E), as compared to HFD control mice. In a PTT, HFD A1L^{-/-} mice increased blood glucose less than HFD control mice (Figure 2F, 2G). It should be noted that differences in insulin sensitivity between the groups can influence glucose output during PTT, without having significant effect on hepatic glucose production. Both HFD A1L^{-/-} and control mice displayed similar sensitivity to glucagon, as shown in a glucagon challenge test (Figure 2H, 2I). Fasting blood glucose levels were decreased in HFD A1L^{-/-} mice, as compared to HFD control littermates (Figure 2J). Fed blood glucose levels were not affected by the lack of hepatocyte A₁AR (Figure 2J). Fasting and fed plasma insulin and glucagon levels were similar between HFD A1L^{-/-} and control mice (Figures 2K, 2L).

3.4. Hyperinsulinemic-euglycemic clamp study with A1L^{-/-} and control mice on HFD

In order to investigate the effect of A₁AR on hepatic glucose fluxes and insulin sensitivity, we conducted hyperinsulinemic-euglycemic clamp studies using isotopically labeled glucose in 5 h-fasted, conscious mice. The control and A1L^{-/-} mice were fed a HFD for 12 weeks

before the clamp studies. The A1L^{-/-} mice showed significantly reduced body weight compared to control mice after 12 weeks on HFD (body weight (g): control: 49.20±1.40; A1L^{-/-}: 45.41±0.94) (Figure 3A). Body composition analysis revealed reduced fat mass in A1L^{-/-} mice (Figure 3B). No difference in lean mass was observed between the groups on HFD (Figure 3B). HFD A1L^{-/-} mice displayed decreased fasting blood glucose levels at the beginning of the clamp study (Figure 3C). Stable euglycemia was achieved in A1L^{-/-} and control mice during 80–120 min (steady state) of the clamp study (Figure 3D). HFD A1L^{-/-} mice showed significantly enhanced glucose infusion rate (GIR), indicating improved insulin sensitivity in A1L^{-/-} compared to the control mice (Figures 3E, 3F). The observed reduced body weight and fat mass may have contributed to the enhanced GIR in A1L^{-/-} mice. Furthermore, plasma insulin levels were decreased in A1L^{-/-} mice in the fasting state, while insulin levels were not significantly different between the groups during the clamp (Figure 3G). No difference was observed between A1L^{-/-} and control mice in the rate of endogenous glucose production (Figure 3H), glycogenolysis (Figure 3I), gluconeogenesis (Figure 3J) during fasting and the clamp study. The rate of glucose disappearance (Rd) was similar in the fasting state (Figure 3K). However, enhanced Rd was observed in A1L^{-/-} mice during the clamp, suggesting improved insulin sensitivity in A1L^{-/-} compared to the control mice (Figure 3K). Supporting the clamp data that hepatic A₁AR does not regulate hepatic glucose fluxes, no difference in mRNA levels of genes involved in hepatic glucose metabolism, such as glucose-6-phosphatase (*G6pc*), phosphoenolpyruvate carboxykinase 1 (*Pck1*), pyruvate dehydrogenase kinase 4 (*Pdk4*), peroxisome proliferator-activated receptor gamma coactivator 1-alpha (*Pgc1a*), glucokinase (*Gck*), and peroxisome proliferator-activated receptor alpha (*Ppara*), was observed in liver of fasting HFD A1L^{-/-} and control mice (Figure 3L). Taken together, the data indicate that liver A₁AR plays a role in regulating whole body insulin sensitivity. However, A₁AR does not regulate liver glucose fluxes under these clamp conditions.

3.5. Insulin sensitivity in A1L^{-/-} and control mice on HFD

To examine the effect of hepatic A₁AR on insulin signaling *in vivo*, we injected insulin (5U) or saline (i.v.) in the inferior vena cava of mice fasted overnight. Liver, adipose tissue and skeletal muscle were dissected 5 min after injection. Western blot analysis revealed that insulin-stimulated phosphorylation of protein kinase B (AKT) at S473 was similar in liver, epididymal white adipose tissue (eWAT), and skeletal muscle isolated from HFD A1L^{-/-} and control mice (Figure 4A–F). It is possible that other depots of fat tissues and skeletal muscles may have contributed to the improved insulin sensitivity observed during ITT and clamp studies.

3.6. HFD A1L^{-/-} mice show no differences in liver steatosis and inflammation

Livers of A1L^{-/-} and control mice were examined after 18 weeks of HFD feeding. The liver mass was similar in A1L^{-/-} and control mice (Figure 5A). Moreover, hepatic triglyceride and glycogen levels were not different between HFD A1L^{-/-} and control mice (Figure 5B, 5C). These data suggest that the hepatocyte A₁AR is not involved in the development of liver steatosis. We also found that hepatocyte A₁AR deficiency did not change the mRNA levels of inflammatory markers in the liver of HFD A1L^{-/-} mice (Figure 5D), suggesting that hepatocyte A₁AR does not play a role in the development of hepatic steatosis.

3.7. $A_1^{-/-} A_3^{-/-}$ mice show similar metabolic profile as control groups on CD

Results with the hepatocyte-specific A_1 AR knockout mouse model revealed that A_1 AR is not essential for the regulation of glucose homeostasis (Figures 1–5). Hence, to understand whether lack of A_1 AR in the whole body regulates glucose metabolism and whether G_i -coupled A_3 AR complements A_1 AR's role in maintaining metabolic homeostasis, we generated four mouse genotypes (WT, $A_1^{-/-}$, $A_3^{-/-}$, $A_1^{-/-} A_3^{-/-}$) as littermates from double heterozygous breeding. These mice were maintained on a CD for 13 weeks post-weaning (4 weeks of age). Lack of either A_1 AR or A_3 AR, or both receptors did not change body weight gain compared to the WT group (Figure 6A). No difference was observed between groups in fed blood glucose levels (Figure 6B). Surprisingly, fasting blood glucose levels were significantly reduced in $A_1^{-/-}$ and $A_1^{-/-} A_3^{-/-}$ compared to the WT mice (Figure 6B). However, plasma insulin levels were not significantly different between the groups under both fasting and fed conditions (Figure 6C). Homeostatic model assessment-insulin resistance (HOMA-IR) was similar between the groups (Figure 6D). No significant difference was observed in glucose tolerance and insulin sensitivity between the groups on CD (Figures 6E–H).

3.8. Metabolic profiling in $A_1^{-/-} A_3^{-/-}$ mice fed with HFD

The potential of A_1 AR and A_3 AR to counteract diet-induced obesity was assessed. After completing metabolic tests on mice maintained on a CD, the mice were transferred to a HFD at 13 weeks of age. The body mass of all four mouse groups was measured weekly for the next 14 weeks. The groups exhibited similar body weight and body composition on a HFD (Figures 7A, B). $A_1^{-/-}$ and $A_1^{-/-} A_3^{-/-}$ mice did not show a difference in fed and fasting blood glucose levels compared to the WT mice (Figure 7C). Also, plasma insulin levels were similar between the mouse groups in fed and fasting states (Figure 7D). HOMA-IR, an estimation of insulin resistance, was found similar between the groups (Figure 7E). These mice were subjected to a series of metabolic tests. Glucose tolerance was not different between WT and $A_1^{-/-} A_3^{-/-}$ or between WT and $A_1^{-/-}$ mice (Figures 7F, G). All four groups of HFD mice showed similar insulin sensitivity in an ITT (Figures 7H, I). $A_1^{-/-} A_3^{-/-}$ mice produced less glucose in a PTT compared to WT mice (Figures 7J, K). Furthermore, the liver weight and hepatic triglyceride levels in $A_1^{-/-}$ and $A_1^{-/-} A_3^{-/-}$ were not significantly different than the WT mice (Figures 7L, M). These data indicate that lack of A_1 AR or double knockout of A_1 AR and A_3 AR in the whole body does not play a significant role in regulating whole body glucose and insulin sensitivity.

4. DISCUSSION

The liver is a key metabolic organ maintaining glucose homeostasis during fasting and fed conditions [33]. In the fed state, glucose is stored as glycogen and converted into fatty acids in the liver [34]. In the fasting state, fuel substrates (glucose and lipids) are released from the liver to be metabolized by extrahepatic tissues. Liver produces and releases glucose during fasting through glycogenolysis and gluconeogenesis [34]. HGP is potently suppressed by insulin under fed conditions. Under conditions of hepatic insulin resistance, insulin is unable to suppress HGP, resulting in hyperglycemia and T2D [33]. In this work, we explored the contribution of the G_i -coupled A_1 AR in the development of hepatic insulin resistance and

glucose fluxes associated with obesity using whole body or hepatocyte-specific knockout. Mice lacking the G_i-coupled A₃AR in addition to the A₁AR were identical in metabolic function to those lacking A₁AR alone.

We selectively ablated A₁AR in mouse hepatocytes (A1L^{-/-}). In vivo studies with A1L^{-/-} mice on a CD showed no significant differences in glucose, insulin, and glucagon tolerance, suggesting no significant role of hepatic A₁AR in regulating metabolism under normal metabolic conditions. Furthermore, to understand the role of hepatic A₁AR, A1L^{-/-} mice were fed a HFD to induce obesity. On HFD, A1L^{-/-} mice showed a slight but significant improvement in whole-body glucose tolerance, insulin sensitivity and pyruvate tolerance. Lack of hepatocyte A₁AR decreased fasting glucose compared to controls. Hyperinsulinemic-euglycemic studies also showed enhanced GIR, a confirmation of improved insulin sensitivity in HFD A1L^{-/-} mice. However, in-vivo insulin sensitivity experiments did not show improved insulin sensitivity in liver, eWAT and the skeletal muscle of HFD A1L^{-/-} mice. The improved insulin sensitivity observed during clamp studies can probably be attributed to indirect effects of hepatic A₁AR on other metabolic tissues involved in maintaining glucose homeostasis. Other G_i-coupled receptors such the CB₁ cannabinoid receptor have been shown to play a key role in liver pathophysiology. Lack of CB₁ in hepatocytes did not change the degree of obesity on HFD, but demonstrated reduced steatosis, hyperglycemia, dyslipidemia and insulin resistance compared to wild type mice [35]. Our data indicate that the hepatic A₁AR does not play a role in improving liver insulin sensitivity. Cross-talk between hepatocytes lacking A₁AR and other metabolic tissues needs to be studied in detail to understand the contribution of other tissues to the observed differences in insulin sensitivity.

Hepatic CB₁R overexpression resulted in increased HGP due to increased glycogenolysis [36]. Involvement of G_i-coupled signaling in HGP regulation was also demonstrated by Rossi et al., in which a G_i-coupled designer GPCR (G_i DREADD) was specifically expressed in hepatocytes [37]. The authors demonstrated that activation of a G_i DREADD specifically in hepatocytes increased HGP, and the lack of functional G_i-protein in hepatocytes reduced blood glucose levels and protected mice against diet-induced metabolic deficits [37]. A₁AR was also reported to enhance glycogenolysis in a Ca²⁺-dependent manner [16]. However, our results indicate that hepatic A₁AR is dispensable for in-vivo HGP as we observed no difference in gluconeogenesis and glycogenolysis in hyperinsulinemic-euglycemic clamp studies with mice on HFD. A modest difference in blood glucose levels observed in HFD mice groups compared to the lean CD fed mice may be due to increased adenosine tone in obesity. Liver cells have been shown to release adenosine and ATP through various mechanisms including ENTs (equilibrative nucleoside transporters), CNTs (concentrative nucleoside transporters), and VNUT (vesicular nucleotide transporter) [38]. The effect of obesity on adenosine release from liver cells should be monitored in the future studies.

In summary, this is the first study exploring the effects of hepatic A₁AR on hepatic insulin resistance and glucose fluxes associated with obesity. We showed that lack of A₁AR specifically in hepatocytes did not affect hepatic glucose fluxes and insulin sensitivity. However, HFD A1L^{-/-} mice displayed decreased fasting glucose levels and

improved whole-body insulin sensitivity. Hence, drugs blocking hepatic A₁AR may improve hyperglycemia associated with metabolic dysfunction and might be explored for the treatment of T2D.

ACKNOWLEDGMENTS

Support from the NIDDK Intramural Research Program (ZIADK31117, ZIADK311129 and ZIADK075063) is acknowledged. We thank Dr. Lu Zhu (NIDDK) for injecting AAV virus into the mouse tail vein, Dr. Huang Yuning (NIDDK) for tagging and tailing mouse groups. Many thanks to Dr. Oksana Gavrilova (Mouse Metabolic Core, NIDDK, NIH) for helpful discussions. Hyperinsulinemic-euglycemic clamps were performed by the Vanderbilt Mouse Metabolic Phenotyping Center (DK059637). The Vanderbilt Hormone Assay and Analytical Core performed the insulin analysis (DK059637 and DK020593).

Abbreviations:

AAV	adeno-associated virus
CD	chow diet
2DG	2-deoxyglucose
EGFP	enhanced green fluorescent protein
eWAT	epididymal white adipose tissue
FFA	free fatty acid
GCT	glucagon challenge test
GIR	glucose infusion rate
GTT	glucagon tolerance test
HFD	high fat diet
HGP	hepatic glucose production
ITT	insulin tolerance test
MPE	molar percent enrichment
NP40	nonyl phenoxypolyethoxylethanol
PTT	pyruvate tolerance test
R_g	glucose metabolic index
TBG	thyroxine-binding globulin

References

1. Postic C, Dentin R, and Girard J, Role of the liver in the control of carbohydrate and lipid homeostasis. *Diabetes Metab*, 2004. 30(5): p. 398–408. [PubMed: 15671906]
2. Moore MC, et al., Regulation of hepatic glucose uptake and storage in vivo. *Adv Nutr*, 2012. 3(3): p. 286–94. [PubMed: 22585902]

3. Sharabi K, et al., Molecular pathophysiology of hepatic glucose production. *Mol Aspects Med*, 2015. 46: p. 21–33. [PubMed: 26549348]
4. Rizza RA, Pathogenesis of fasting and postprandial hyperglycemia in type 2 diabetes: implications for therapy. *Diabetes*, 2010. 59(11): p. 2697–707. [PubMed: 20705776]
5. Basu R, et al., Pathogenesis of prediabetes: role of the liver in isolated fasting hyperglycemia and combined fasting and postprandial hyperglycemia. *J Clin Endocrinol Metab*, 2013. 98(3): p. E409–17. [PubMed: 23345093]
6. Sarwar R, Pierce N, and Koppe S, Obesity and nonalcoholic fatty liver disease: current perspectives. *Diabetes Metab Syndr Obes*, 2018. 11: p. 533–542. [PubMed: 30288073]
7. Luyckx FH, Lefebvre PJ, and Scheen AJ, Non-alcoholic steatohepatitis: association with obesity and insulin resistance, and influence of weight loss. *Diabetes Metab*, 2000. 26(2): p. 98–106. [PubMed: 10804323]
8. Fredholm BB, et al., International Union of Pharmacology. XXV. Nomenclature and classification of adenosine receptors. *Pharmacol Rev*, 2001. 53(4): p. 527–52. [PubMed: 11734617]
9. Fredholm BB, et al., International Union of Basic and Clinical Pharmacology. LXXXI. Nomenclature and classification of adenosine receptors--an update. *Pharmacol Rev*, 2011. 63(1): p. 1–34. [PubMed: 21303899]
10. Grden M, et al., Diabetes-induced alterations of adenosine receptors expression level in rat liver. *Exp Mol Pathol*, 2007. 83(3): p. 392–8. [PubMed: 17490639]
11. Johnston-Cox H, et al., The A2b adenosine receptor modulates glucose homeostasis and obesity. *PLoS One*, 2012. 7(7): p. e40584. [PubMed: 22848385]
12. Csoka B, et al., A2B adenosine receptors prevent insulin resistance by inhibiting adipose tissue inflammation via maintaining alternative macrophage activation. *Diabetes*, 2014. 63(3): p. 850–66. [PubMed: 24194503]
13. Yip L, et al., Diminished adenosine A1 receptor expression in pancreatic alpha-cells may contribute to the pathology of type 1 diabetes. *Diabetes*, 2013. 62(12): p. 4208–19. [PubMed: 24264405]
14. Jain S and Jacobson KA, Purinergic signaling in diabetes and metabolism. *Biochem Pharmacol*, 2020: p. 114393. [PubMed: 33359363]
15. McLane MP, et al., Adenosine reversal of in vivo hepatic responsiveness to insulin. *Diabetes*, 1990. 39(1): p. 62–9. [PubMed: 2210062]
16. Gonzalez-Benitez E, et al., Regulation of glycogen metabolism in hepatocytes through adenosine receptors. Role of Ca²⁺ and cAMP. *Eur J Pharmacol*, 2002. 437(3): p. 105–11. [PubMed: 11890897]
17. Peng Z, et al., Adenosine signaling contributes to ethanol-induced fatty liver in mice. *J Clin Invest*, 2009. 119(3): p. 582–94. [PubMed: 19221436]
18. Scammell TE, et al., Focal deletion of the adenosine A1 receptor in adult mice using an adeno-associated viral vector. *J Neurosci*, 2003. 23(13): p. 5762–70. [PubMed: 12843280]
19. Salvatore CA, et al., Disruption of the A(3) adenosine receptor gene in mice and its effect on stimulated inflammatory cells. *J Biol Chem*, 2000. 275(6): p. 4429–34. [PubMed: 10660615]
20. Sun D, et al., Mediation of tubuloglomerular feedback by adenosine: evidence from mice lacking adenosine 1 receptors. *Proc Natl Acad Sci U S A*, 2001. 98(17): p. 9983–8. [PubMed: 11504952]
21. Carlin JL, et al., Hypothermia in mouse is caused by adenosine A1 and A3 receptor agonists and AMP via three distinct mechanisms. *Neuropharmacology*, 2017. 114: p. 101–113. [PubMed: 27914963]
22. Jain S, et al., Adipocyte P2Y14 receptors play a key role in regulating whole-body glucose and lipid homeostasis. *JCI Insight*, 2021. 6(10).
23. Berglund ED, et al., Glucose metabolism in vivo in four commonly used inbred mouse strains. *Diabetes*, 2008. 57(7): p. 1790–9. [PubMed: 18398139]
24. Ayala JE, et al., Considerations in the design of hyperinsulinemic-euglycemic clamps in the conscious mouse. *Diabetes*, 2006. 55(2): p. 390–7. [PubMed: 16443772]

25. Hasenour CM, et al., Mass spectrometry-based microassay of (2)H and (13)C plasma glucose labeling to quantify liver metabolic fluxes in vivo. *Am J Physiol Endocrinol Metab*, 2015. 309(2): p. E191–203. [PubMed: 25991647]
26. Hughey CC, et al., Loss of hepatic AMP-activated protein kinase impedes the rate of glycogenolysis but not gluconeogenic fluxes in exercising mice. *J Biol Chem*, 2017. 292(49): p. 20125–20140. [PubMed: 29038293]
27. Steele R, et al., Measurement of size and turnover rate of body glucose pool by the isotope dilution method. *Am J Physiol*, 1956. 187(1): p. 15–24. [PubMed: 13362583]
28. Burgess SC, et al., Impaired tricarboxylic acid cycle activity in mouse livers lacking cytosolic phosphoenolpyruvate carboxykinase. *J Biol Chem*, 2004. 279(47): p. 48941–9. [PubMed: 15347677]
29. Antoniewicz MR, Kelleher JK, and Stephanopoulos G, Measuring deuterium enrichment of glucose hydrogen atoms by gas chromatography/mass spectrometry. *Anal Chem*, 2011. 83(8): p. 3211–6. [PubMed: 21413777]
30. Kraegen EW, et al., Dose-response curves for in vivo insulin sensitivity in individual tissues in rats. *Am J Physiol*, 1985. 248(3 Pt 1): p. E353–62. [PubMed: 3883806]
31. Pydi SP, et al., beta-arrestin-1 suppresses myogenic reprogramming of brown fat to maintain euglycemia. *Sci Adv*, 2020. 6(23): p. eaba1733. [PubMed: 32548266]
32. Jain S, et al., Lack of adipocyte purinergic P2Y6 receptor greatly improves whole body glucose homeostasis. *Proc Natl Acad Sci U S A*, 2020.
33. Roden M and Shulman GI, The integrative biology of type 2 diabetes. *Nature*, 2019. 576(7785): p. 51–60. [PubMed: 31802013]
34. Rui L, Energy metabolism in the liver. *Compr Physiol*, 2014. 4(1): p. 177–97. [PubMed: 24692138]
35. Osei-Hyiaman D, et al., Hepatic CB1 receptor is required for development of diet-induced steatosis, dyslipidemia, and insulin and leptin resistance in mice. *J Clin Invest*, 2008. 118(9): p. 3160–9. [PubMed: 18677409]
36. Liu J, et al., Hepatic cannabinoid receptor-1 mediates diet-induced insulin resistance via inhibition of insulin signaling and clearance in mice. *Gastroenterology*, 2012. 142(5): p. 1218–1228 e1. [PubMed: 22307032]
37. Rossi M, et al., Hepatic Gi signaling regulates whole-body glucose homeostasis. *J Clin Invest*, 2018. 128(2): p. 746–759. [PubMed: 29337301]
38. Jain S, Jacobson KA, Purinergic signaling in liver pathophysiology. *Frontiers in Endocrinology*, 2021. 12.

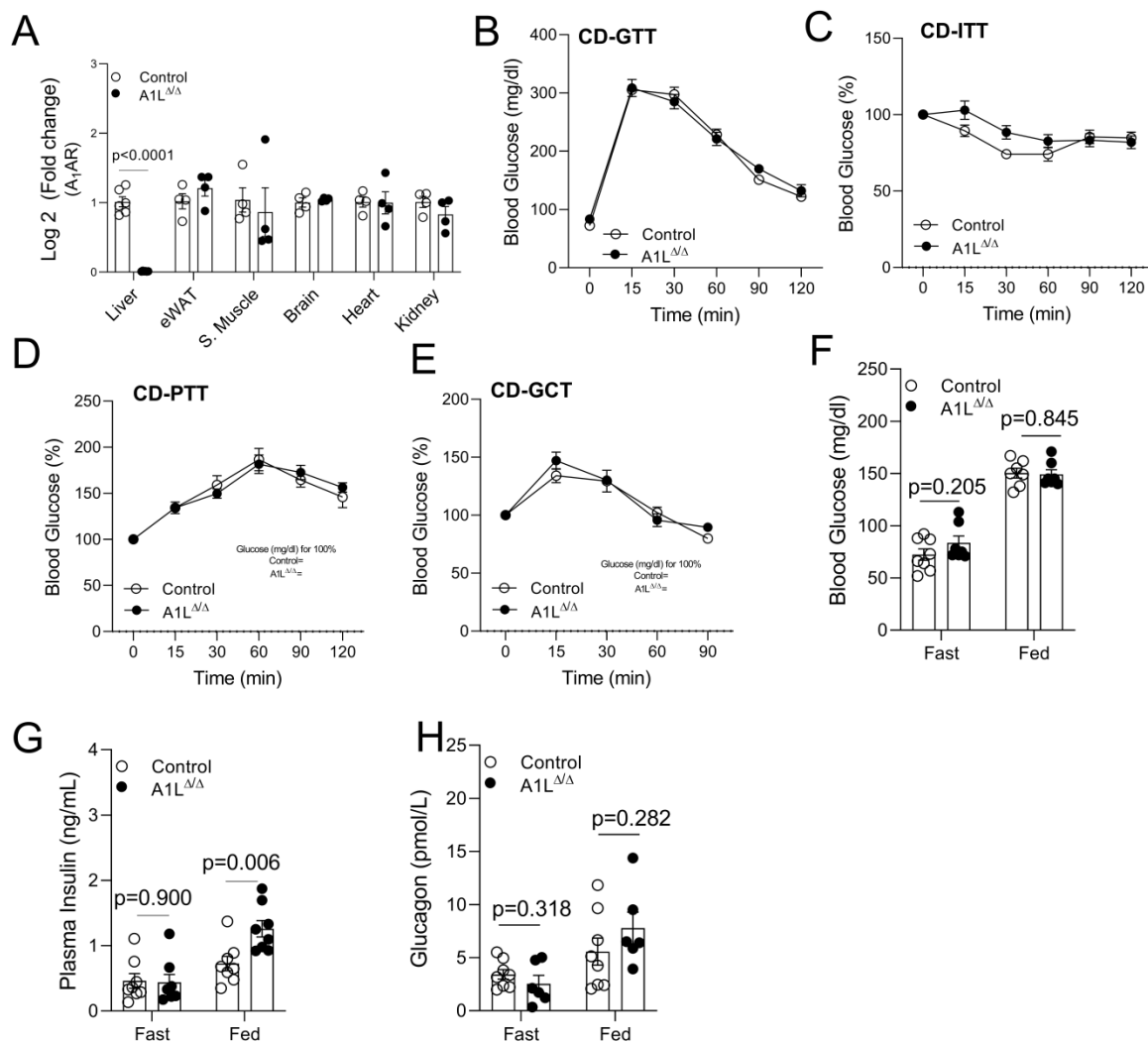


Figure 1. Metabolic analysis of hepatocyte-specific A_1AR knockout ($A1L^{\Delta/\Delta}$) mice maintained on CD.

(A) RT-PCR analysis of A_1AR mRNA levels in liver and other tissue of control and $A1L^{\Delta/\Delta}$ mice (n=4–6/group).

(B) Glucose tolerance tests (2 g glucose/kg, i.p.; GTT) performed with control and $A1L^{\Delta/\Delta}$ mice.

(C) Insulin tolerance tests (0.75 U insulin/kg, i.p.; ITT) carried out with control and $A1L^{\Delta/\Delta}$ mice. Glucose (mg/dl) at 0 min – control: 132.8 ± 8.11 , $A1L^{\Delta/\Delta}$: 135.9 ± 8.99 .

(D) Pyruvate tolerance tests (2 g sodium pyruvate/kg, i.p.; PTT). Glucose (mg/dl) at 0 min – control: 83.71 ± 6.89 , $A1L^{\Delta/\Delta}$: 97.43 ± 7.03 .

(E) Glucagon tolerance tests (16 μ g glucagon/kg, i.p.; GCT). Glucose (mg/dl) at 0 min – control: 140.3 ± 6.1 , $A1L^{\Delta/\Delta}$: 113.0 ± 6.8 .

(F) Fasting and fed blood glucose levels.

(G) Fasting and fed plasma insulin levels.

(H) Fasting and fed plasma glucagon levels.

Data represent the mean \pm SEM (B-H) (n=6–8/group).

18s rRNA was used as normalization control for RT-PCR analysis. Statistical significance was determined (A, F–H) with the two-tailed Student's *t* test. (B–E) 2-way ANOVA followed by Bonferroni's multiple comparison's test.

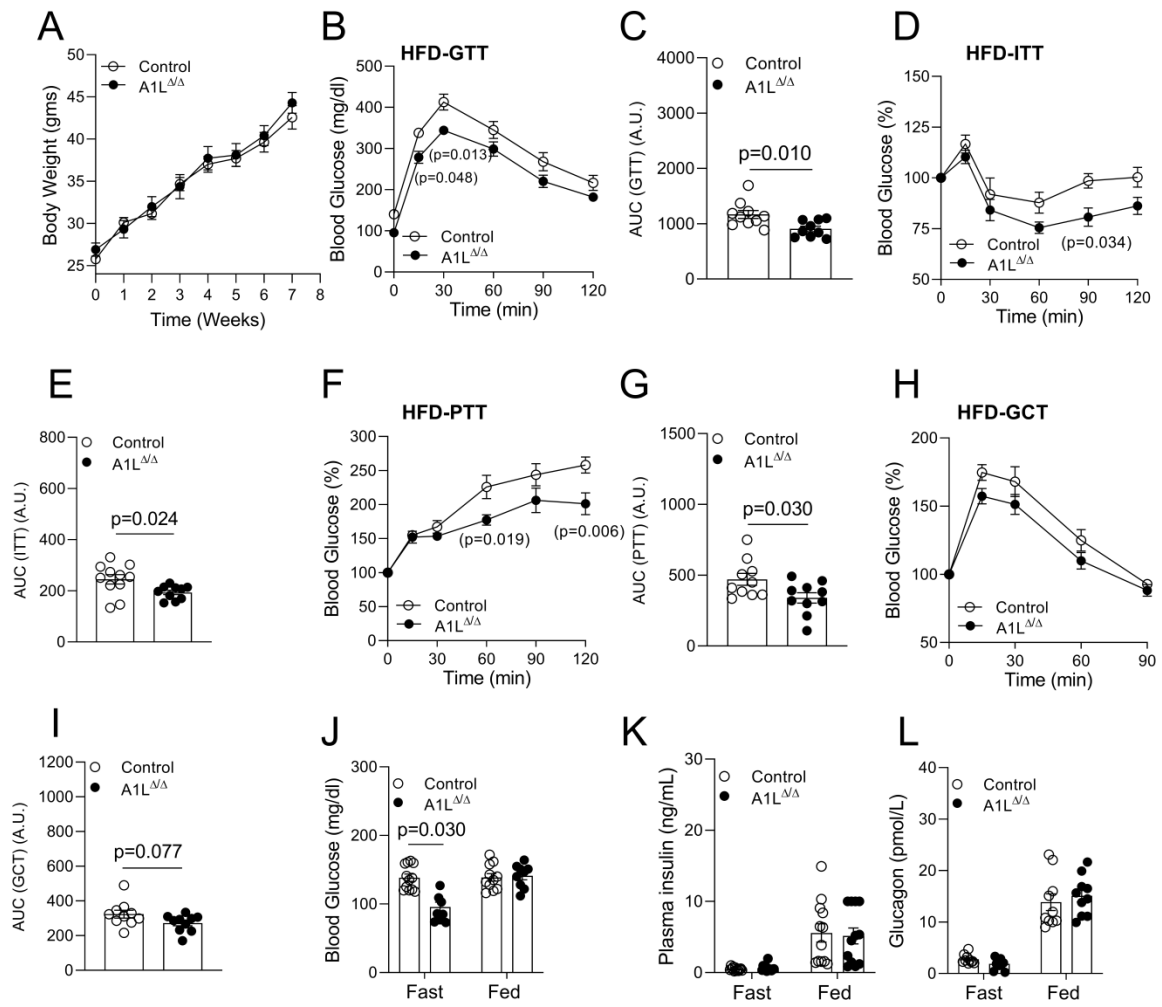


Figure 2. Metabolic analysis of A1L^{-/-} mice on HFD.

(A) Body weight gain in A1L^{-/-} and control mice on HFD for 7 weeks.

(B) Glucose tolerance tests (1 g glucose/kg, i.p.; GTT) performed with control and A1L^{-/-} mice.

(C) The AUC (A.U.) for GTT.

(D) Insulin tolerance tests (1 U insulin/kg, i.p.; ITT) carried out with control and A1L^{-/-} mice. Glucose (mg/dl) at 0 min – control:173.2±26.5, A1L^{-/-}:185.0±25.1.

(E) The AUC (A.U.) for ITT.

(F) Pyruvate tolerance tests (2 g sodium pyruvate/kg, i.p.; PTT). Glucose (mg/dl) at 0 min – control:157.0±13.1, A1L^{-/-}:150.8±16.3.

(G) The AUC (A.U.) for PTT.

(H) Glucagon tolerance tests (16 µg glucagon/kg, i.p.; GCT). Glucose (mg/dl) at 0 min – control:175.6±14.9, A1L^{-/-}:159.3±11.6.

(I) The AUC (A.U.) for GCT.

(J) Fasting and fed blood glucose levels.

(K) Fasting and fed plasma insulin levels.

(L) Fasting and fed plasma glucagon levels.

Data represent the mean \pm SEM (n= 9–11 per group. Statistical significance was determined (A, C, E, G, I–L) with the two-tailed Student's *t* test. (B, D, F, H) 2-way ANOVA followed by Bonferroni's multiple comparison's test.

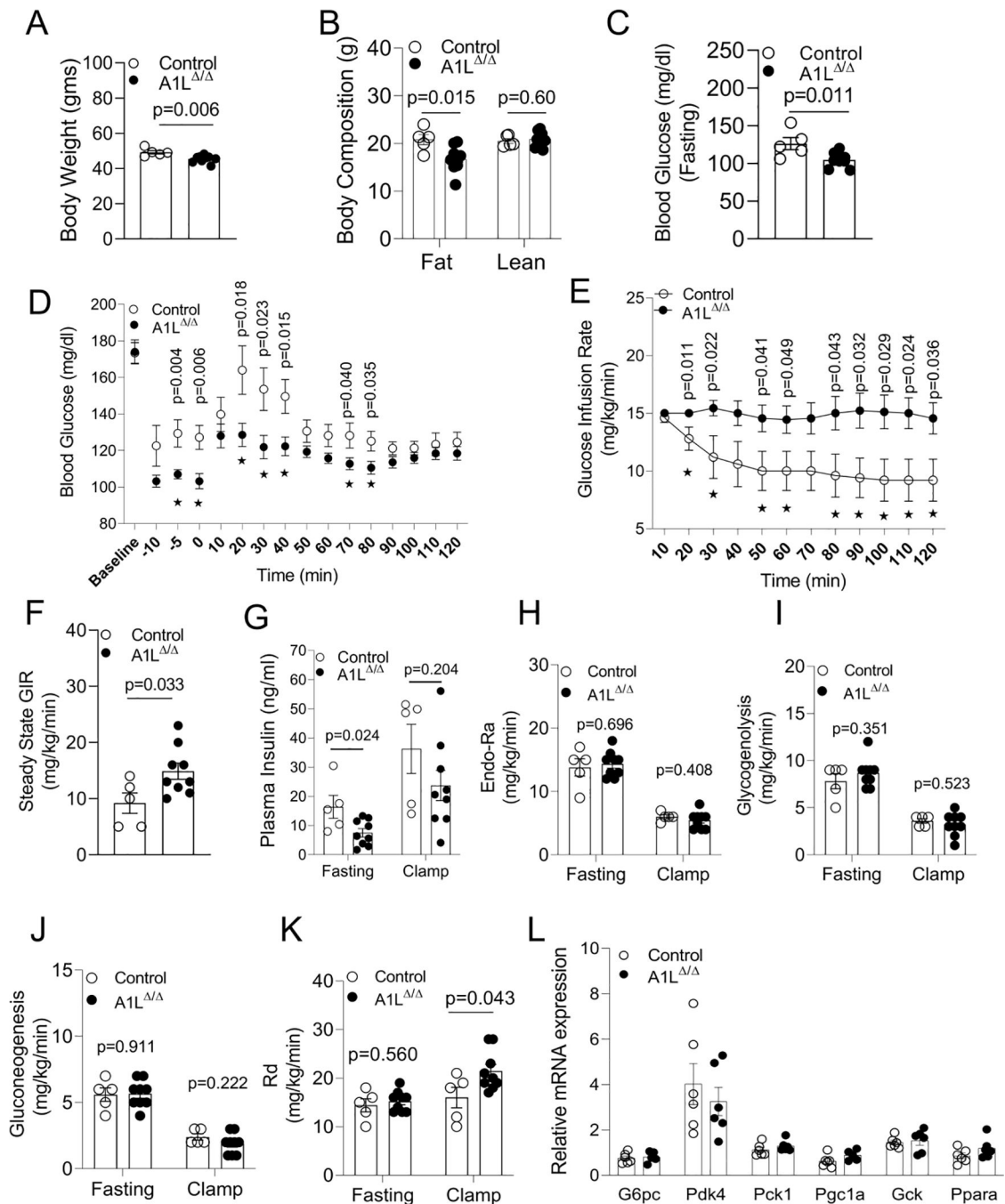


Figure 3. Hyperinsulinemic-euglycemic studies on HFD A1L^{Δ/Δ} mice.

(A) Body weight of control and A1L^{Δ/Δ} mice used for the clamp study.

(B) Body composition (fat and lean mass) of control and A1L^{Δ/Δ} mice.

(C) Fasting blood glucose levels in control and A1L^{Δ/Δ} mice before starting the clamp study.

(D) Time course of arterial blood glucose levels.

(E) Glucose infusion rate (GIR).

(F) GIR during steady state duration (80–120 min) of the clamp.

(G) Plasma insulin levels during fasting and clamp study.

(H) Endogenous glucose production (Endo-Ra).

(I) Glycogenolysis rate.

(J) Gluconeogenesis rate.

(K) Rate of blood glucose clearance (Rd) during the fasting (basal state) and clamp study.

(L) mRNA expression levels of genes (G6pc, Pdk4, Pck1, Pgc1a, Gck and, Ppara) involved in glucose metabolism in the liver tissues of fasted control and A1L^{-/-} mice.

Data represent the mean \pm SEM (A-K: n= 9–11 per group, L: 5–6 per group). 18s rRNA was used as normalization control for RT-PCR analysis. Statistical significance was determined with the two-tailed Student's *t* test.

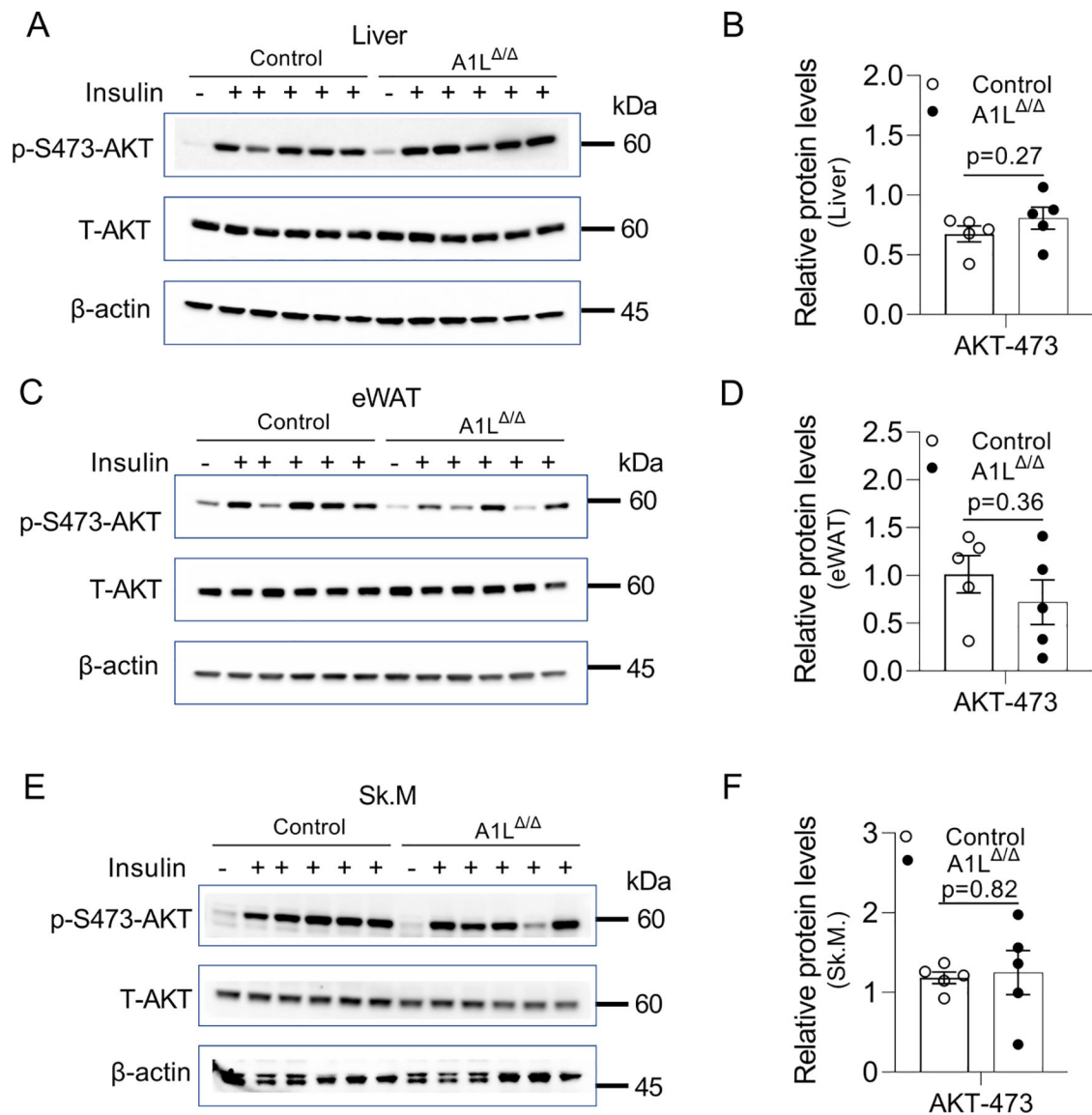


Figure 4. Insulin signaling in HFD A1L^{-/-} mice compared to WT control mice. Insulin (5U in 100 μ l) or saline was injected (i.v.) into the vena cava of anesthetized mice. Tissues were collected 5 min after injection. (A-F) Western blot analysis of insulin signaling in (A) liver, (C) eWAT, (E) skeletal muscle of HFD adipo-A1L^{-/-} and control mice (n=5/group). Quantification of immunoblotting data is shown in (B) liver, (D) eWAT, and (F) skeletal muscle (n=5/group). Data represent the mean \pm SEM. Statistical significance was determined with the two-tailed Student's *t* test.

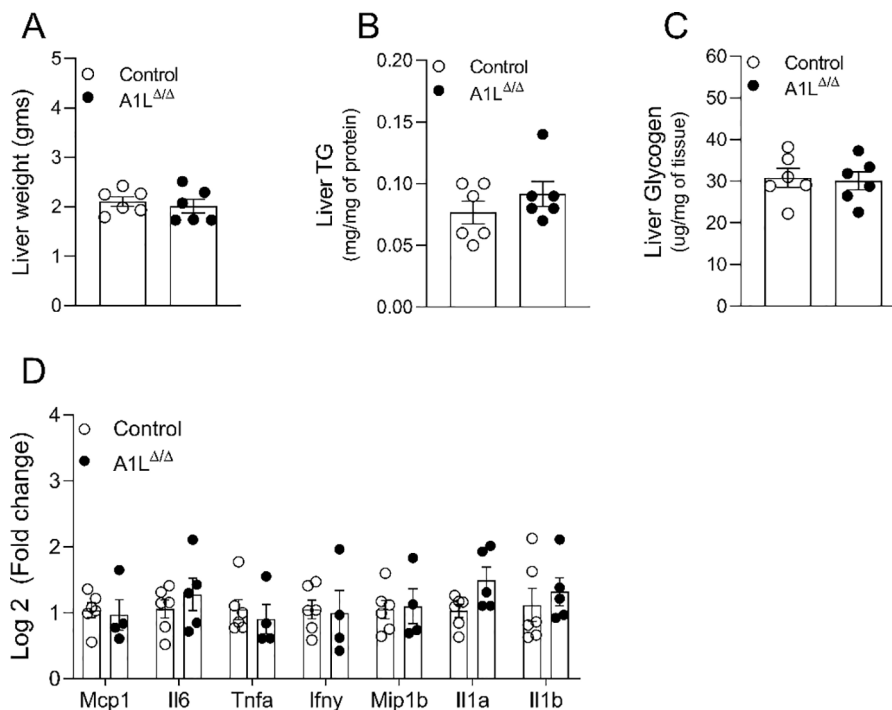


Figure 5. Liver metabolism in A1L^{-/-} mice consuming a HFD for 18 weeks.

(A) Liver weight (in g) of control and A1L^{-/-} mice (n= 6 per group).

(B) Liver triglyceride levels in control and A1L^{-/-} mice (n= 6 per group).

(C) Liver glycogen levels in control and A1L^{-/-} mice (n= 6 per group).

(D) RT-PCR analysis of inflammatory markers in the liver of A1L^{-/-} and control mice (n= 4–6 per group).

Data represent the mean \pm SEM. Statistical significance was determined with the two-tailed Student's *t* test. 18s rRNA was used as normalization control for the RT-PCR analysis.

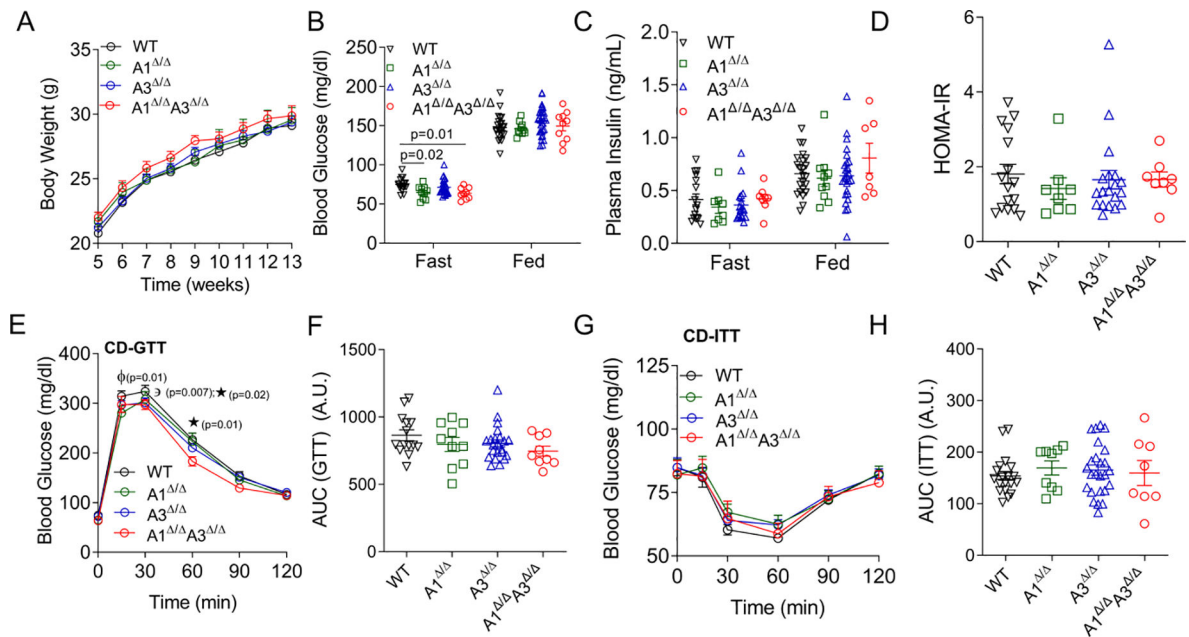


Figure 6. A1^{-/-} A3^{-/-} mice show no major changes in metabolism on regular chow diet (CD).

(A) Body weight gain of controls and A1^{-/-} A3^{-/-} mice consuming CD.

(B) Fasting and fed blood glucose levels.

(C) Fasting and fed plasma insulin levels.

(D) Homeostatic model assessment-insulin resistance (HOMA-IR) between the groups.

(E) Glucose tolerance tests (2 g glucose/kg, i.p.; GTT) between controls and A1^{-/-} A3^{-/-} mice.

(F) The AUC for GTT.

(G) Insulin tolerance tests (0.75 U insulin/kg, i.p.; ITT) between controls and A1^{-/-} A3^{-/-} mice.

(H) The AUC for ITT.

All experiments were performed on male mice more than 10 weeks of age. Data represent the mean \pm SEM (WT and A3^{-/-} : n= 15–20 per group, A1^{-/-} and A1^{-/-} A3^{-/-} : n= 7–10 per group). **P*. (WT and A1^{-/-} A3^{-/-}), ϕ *P*. (WT and A1^{-/-}), ϑ *P*. (WT and A3^{-/-}). Statistical significance was determined (A, E and G) 2-way ANOVA followed by Bonferroni's multiple comparison's test; (B–D, F and H) 1-way ANOVA followed by Bonferroni's multiple comparison's test. Post-hoc calculation was conducted, power was >50% where p-value was reported as <0.05.

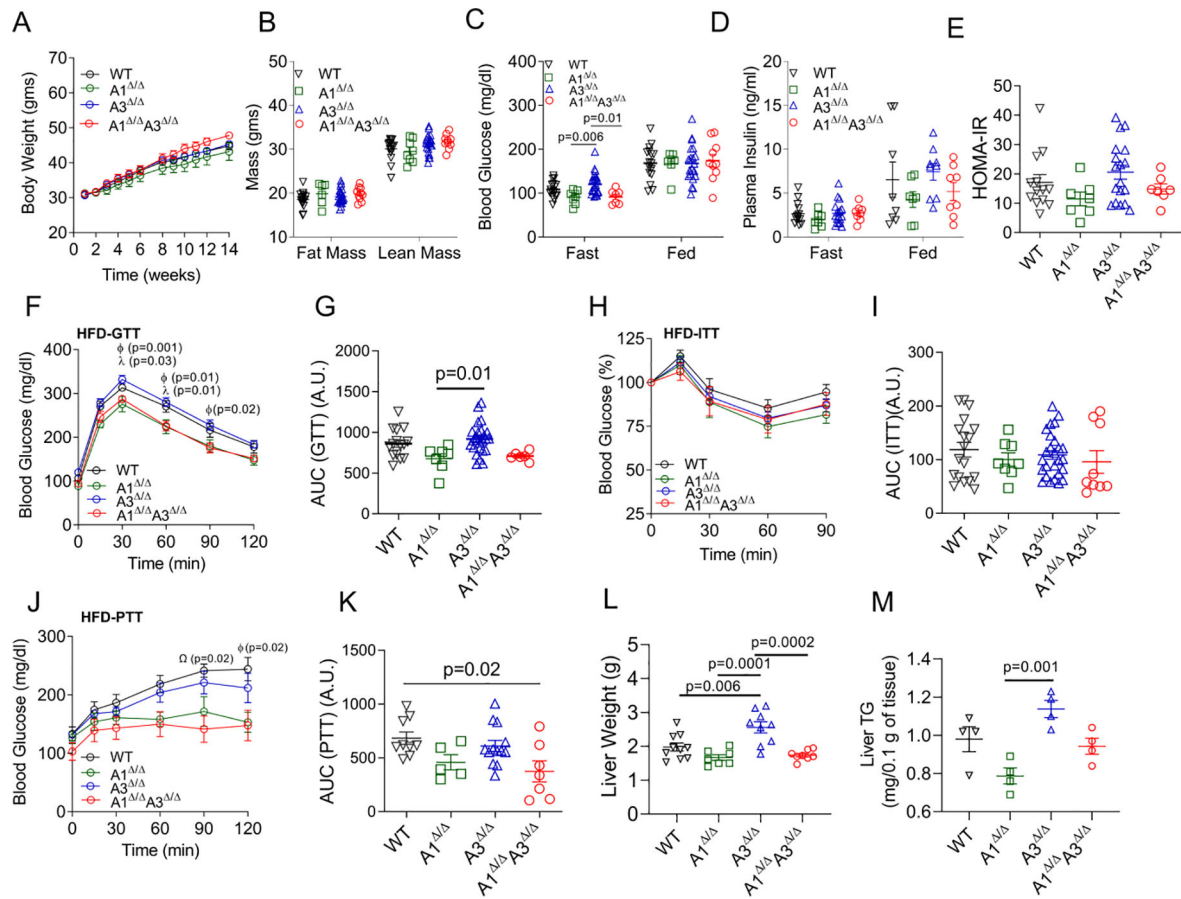


Figure 7. Effect on obesity and glucose metabolism in $A1^{-/-} A3^{-/-}$ mice fed with a HFD.

(A) Body weight gain of control and $A1^{-/-} A3^{-/-}$ mice consuming HFD.

(B) Body composition of mice maintained on HFD.

(C) Fasting and fed blood glucose levels

(D) Fasting and fed plasma insulin levels.

(E) HOMA-IR in control and knockout mice on HFD.

(F) Glucose tolerance tests (1 g glucose/kg, i.p.; GTT).

(G) The AUC for GTT.

(H) Insulin tolerance tests (1 U insulin/kg, i.p.; ITT). Glucose (mg/dl) at 0 min – WT: 105.0 ± 10.9 ; $A1^{-/-}$: 94.83 ± 10.61 ; $A3^{-/-}$: 112.5 ± 8.7 ; $A1^{-/-} A3^{-/-}$: 93.29 ± 10.37 .

(I) The AUC for ITT.

(J) Pyruvate tolerance tests (2 g sodium pyruvate/kg, i.p.; PTT) between the groups.

(K) The AUC for PTT.

(L) Liver weight (grams) in control and $A1^{-/-} A3^{-/-}$ mice. (n=8–10/group).

(M) Liver triglyceride levels in control and $A1^{-/-} A3^{-/-}$ mice. (n=4/group).

Data represent the mean \pm SEM (WT and $A3^{-/-}$: n= 15–20 per group, $A1^{-/-}$ and $A1^{-/-} A3^{-/-}$: n= 7–8 per group). ϕ P: ($A3^{-/-}$ and $A1^{-/-} A3^{-/-}$); λ P: ($A3^{-/-}$ and $A1^{-/-}$).

For PTT, ω P: (WT and $A1^{-/-} A3^{-/-}$); ϕ P: (WT and $A1^{-/-}$). Statistical significance was determined (A, F, H and J) by 2-way ANOVA followed by Bonferroni's multiple comparison's test; (B–E, G, I, K–M) 1-way ANOVA followed by Bonferroni's multiple

comparison's test. Post-hoc calculation was conducted, power was >50% where p-value was reported as <0.05.

Table 1.

PCR primers (mouse) used for qRT-PCR experiments.

Gene name	Forward (5'–3')	Reverse (5'–3')
18S rRNA	CGGCTACCACATCCAAGGAA	GCTGGAATTACCGCGGCT
<i>G6pc</i>	CGACTCGCTATCTCCAAGTGA	GTTGAACCAGTCTCCGACCA
<i>Tnfa</i>	CCCTCACACTCAGATCATCTTCT	GCTACGACGTGGGCTACAG
<i>IFNy</i>	CGGCACAGTCATTGAAAGCCTA	GTTGCTGATGGCCTGATTGTC
<i>IL-1a</i>	ACGTCAAGCAACGGGAAGAT	AAGGTGCTGATCTGGGTTGG
<i>IL-1b</i>	CTCCACCTCAATGGACAGAA	GCCGTCTTTCATTACACAGG
<i>IL6</i>	TAGTCCTTCTACCCCAATTCC	TTGGTCCTTAGCCACTCCTTC
<i>Mcp1</i>	GCTCAGCCAGATGCAGTTAA	TCTTGAGCTTGGTGACAAAAACT
<i>Mip1b</i>	AACAACATGAAGCTCTGCGT	AGAAACAGCAGGAAGTGGGA
<i>Pck1</i>	CTGCATAACGGTCTGGACTTC	CAGCAACTGCCCGTACTCC
<i>Pdk4</i>	CCGCTTAGTGAACACTCCTTC	TGACCAGCGTGTCTACAAACT
<i>Pgc1a</i>	AGCCGTGACCACTGACAAC GAG	GCTGCATGGTTCTGAGTGCTAAG
<i>Ppara</i>	GCGTACGGCAATGGCTTTAT	GAACGGCTTCTCAGGTTCTT
<i>Gck</i>	ATGGCTGTGGATACTACAAGGA	TTCAGGCCACGGTCCATCT
<i>AIAR</i>	CCCCATCGTCTATGCCTTCC	CATCGGAAGTGGTCGTTCCA